NeuroImage 62 (2012) 1390–1398

Contents lists available at SciVerse ScienceDirect

NeuroImage

journal homepage: www.elsevier.com/locate/ynimg

Quantitative MR imaging of two-pool magnetization transfer model parameters in myelin mutant *shaking* pup

Alexey Samsonov [a,*], Andrew L. Alexander [b,c,d], Pouria Mossahebi [e], Yu-Chien Wu [b,f], Ian D. Duncan [g], Aaron S. Field [a,e]

[a] Department of Radiology, University of Wisconsin-Madison, Madison, WI, USA
[b] Waisman Laboratory for Brain Imaging and Behavior, University of Wisconsin-Madison, Madison, WI, USA
[c] Department of Medical Physics, University of Wisconsin-Madison, Madison, WI, USA
[d] Department of Psychiatry, University of Wisconsin-Madison, Madison, WI, USA
[e] Department of Biomedical Engineering, University of Wisconsin-Madison, Madison, WI, USA
[f] Dartmouth Brain Imaging Center, Dartmouth College, Hanover, NH, USA
[g] Department of Medical Sciences, School of Veterinary Medicine, University of Wisconsin-Madison, Madison, WI, USA

ARTICLE INFO

Article history:
Accepted 28 May 2012
Available online 1 June 2012

Keywords:
Quantitative magnetization transfer
Cross-relaxation imaging
White matter
Myelin
Animal models
Relaxometry

ABSTRACT

Magnetization transfer (MT) imaging quantitatively assesses cerebral white matter disease through its sensitivity to macromolecule-bound protons including those associated with myelin proteins and lipid bilayers. However, traditional MT contrast measured by the MT ratio (MTR) lacks pathologic specificity as demyelination, axon loss, inflammation and edema all impact MTR, directly and/or indirectly through multiple covariances among imaging parameters (particularly MTR with T_1) and tissue features (e.g. axon loss with demyelination). In this study, more complex modeling of MT phenomena ("quantitative" MT or qMT) was applied to a *less* complex disease model (the myelin mutant *shaking* [*sh*] pup, featuring hypomyelination but neither inflammation nor axon loss) in order to eliminate the covariances on both sides of the MR-pathology "equation" and characterize these important relationships free from the usual confounds. qMT measurements were acquired longitudinally in 6 *sh* pups and 4 age-matched controls ranging from 3 to 21 months of age and compared with histology. The qMT parameter, bound pool fraction (f), was the most distinctive between diseased and control animals; both f and longitudinal relaxation rate R_1 tracked myelination with normal aging, whereas MTR did not—presumably owing to counterbalancing MT and R_1 effects. qMT imaging provides a more accurate and potentially more specific non-invasive tissue characterization.

Introduction

Non-invasive assessment of white matter (WM) status by magnetic resonance imaging (MRI) plays an important role in the diagnosis and assessment of disease burden in a variety of diseases of the central nervous system (CNS). Unfortunately, conventional MRI methods based on T_1, T_2 and proton density (*PD*) image contrast have relatively low sensitivity and even lower specificity to neuropathology. For example, in multiple sclerosis (MS), myelin loss, axon damage, inflammation, macrophage infiltration and edema all contribute to the image contrasts. This lack of specificity impedes the progress of clinical research in a host of potentially treatable WM diseases by making it difficult or impossible to track the neuropathologic process before, during and after therapeutic intervention.

Several advanced MRI methods such as diffusion tensor imaging (DTI) (Pierpaoli et al., 1996), magnetization transfer imaging (MTI) (Wolff and Balaban, 1989) and multicomponent relaxometry (MacKay et al., 1994) are promising not only to visualize the pathology but also to allow more specific, quantitative assessment of the pathological substrates of the disease. Among these methods, MTI is sensitive to immobile, bound protons immeasurable by conventional MRI, such as those associated with the macromolecules in proteins and lipid bilayers of myelin. Still, traditional magnetization transfer contrast as measured by the magnetization transfer ratio (MTR) is a nonspecific indicator of underlying pathology. Myelin loss, axon damage, macrophage infiltration and edema (Deloire-Grassin et al., 2000; Dousset et al., 1995; Gass et al., 1994; Kimura et al., 1996; Loevner et al., 1995; van Waesberghe et al., 1999) all contribute to MT contrast. As one possible solution to improve the sensitivity, specificity, and reproducibility of MT metrics, more complex modeling of MT phenomena ("quantitative" MT or qMT) has been proposed (Gochberg and Gore, 2003; Gochberg et al., 1999; Ropele et al., 2003). Several investigators have adapted a two-pool model of MT for in vivo measurements (Sled and Pike, 2001; Tozer

* Corresponding author at: Department of Radiology, University of Wisconsin-Madison, WIMR, 1111 Highland Dr, Rm. 1117, Madison, WI 53705, USA. Fax: +1 608 265 9840.
E-mail address: samsonov@wisc.edu (A. Samsonov).

1053-8119/$ – see front matter © 2012 Elsevier Inc. All rights reserved.
doi:10.1016/j.neuroimage.2012.05.077

et al., 2003; Yarnykh, 2002; Yarnykh and Yuan, 2004). In this model, macromolecular protons (bound pool) are considered in magnetization exchange with free water protons (free pool). The parameters of the two-pool model include the bound pool fraction (f, the ratio of protons bound to macromolecules to the total number of protons), cross-relaxation rate constant (k, the rate of magnetization exchange between the free and bound pools), T_2 of the bound pool (T_{2b}), and longitudinal relaxation rate (R_1) of the free pool. Several initial studies have revealed potential clinical significance of qMT measures, such as their relevance to the clinical disability of MS patients, the ability to track myelination (Davies et al., 2004), and sensitivity to lesions not visible on T_1-weighted scans (Levesque et al., 2005). The measures were sensitive to tissue composition manifested as regional variations in WM of the brain (Sled and Pike, 2001) and provided information about fiber tracts independent from DTI (Stikov et al., 2011; Underhill et al., 2009).

The bound pool fraction f is thought to be the key qMT measure and its sensitivity to myelin has been investigated in several studies. Schmierer et al. (2007) found significant correlation between myelin content and f in human MS brain post mortem. Bound pool fraction also was significantly correlated with myelin water fraction (MWF), another measure of myelin content, in human brain post mortem (Tozer et al., 2005). Bound pool fraction was a robust measure of bulk myelin content in histological studies of excised and fixed rat spinal cords (Dula et al., 2010). Strong correlation of f with myelin density also was found in healthy rat brains (Underhill et al., 2011). However, while in healthy WM bound pool fraction is dominated by myelin (Kucharczyk et al., 1994), histological (Norton and Autilio, 1966) and imaging (Bjarnason et al., 2005; Ou et al., 2009a, 2009b) studies suggest that it also may be significantly modulated by other components of semisolids, such as axonal membranes and other macromolecules existing even in non-myelinated tissues (Levesque and Pike, 2009). Studying the specificity of qMT measures, however, presents several practical challenges. Coupling between different pathological substrates in diseased tissues often precludes disentangling the complex relationships between qMT measures and tissue microenvironment. For example, in addition to demyelination, the effect of other pathologic changes such as inflammation on qMT measures has to be considered (Odrobina et al., 2005). In normal tissues, there is limited opportunity to probe tissues with significantly different levels of compartmentalization (for example, normally myelinated vs. near completely demyelinated WM) to derive informative correlations between qMT measures and microstructural features. For example, axon status may potentially affect MT measures sensitive to demyelination. Traditional MTR strongly correlated both with demyelination and axon loss in post mortem studies of MS spinal cord (Mottershead et al., 2003). At the same time, MTR was found insensitive to axon loss in serial optic neuritis studies (Hickman et al., 2004), which was attributed to opposing effects of confounding pathologies on MTR. Schmierer et al. (2007) found significant correlation not only between f and myelin content but also between myelin content and axon count in post mortem MS brain. In all these studies, the effects of myelin and axon status on MT measures were confounded.

Obviously, interpretation of MT measures may greatly benefit from the ability to modify pathological effects in controlled fashion and/or from studying abnormal tissues with significantly modified proton pool sizes. Hence, animal models with acquired or inherited disorders of CNS white matter have been important to study associations of MT parameters with microstructural integrity (Ou et al., 2009a, 2009b; Rausch et al., 2009). For example, in nonhuman primates with experimental autoimmune encephalomyelitis (EAE, an animal model of multiple sclerosis) Blezer et al., (2007) found no significant correlation between axon density and MTR. In another study, Ou et al. (2009b) used retinal ischemia to induce axonal injury without detectable demyelination in optic nerves of control and *shiverer* (myelin deficient) mice, finding that the pool size ratio P, an alternative measure of bound proton content ($f = P/(P+1)$) with proven sensitivity to myelin (Dula et al., 2010; Schmierer et al., 2007; Underhill et al., 2011), was not significantly affected by axonal injury (Ou et al., 2009b). Note that *insensitivity to axons* is a necessary, but not sufficient, condition for a parameter to be a specific myelin marker. It is unclear how semisolid components other than axonal membranes and myelin affect bound pool fraction.

In this paper, we report results of studying two-pool-model MT measures across ages in the *shaking* (*sh*) pup, one of the "myelin mutants" and an animal model of Pelizaeus–Merzbacher disease (PMD), the dysmyelinating disorder in humans. The *sh* pup is a well-studied canine mutant with a profound paucity of myelin, without the confounding effects of axonal loss, inflammation and gliosis (Bray et al., 1983; Duncan et al., 1983; Griffiths et al., 1981a, 1981b). The *sh* pup is characterized by severe hypomyelination throughout the CNS (Figs. 1a,b), caused by a point mutation in the myelin proteolipid protein (PLP) gene (Nadon et al., 1990) that hinders the development of mature oligodendrocytes. The production of PLP and myelin basic protein is considerably reduced in the *sh* pup (Nadon and Duncan, 1996). Axons in the *sh* pup CNS at any age are either non-myelinated or surrounded by a disproportionately thin layer of myelin compared to normal (Figs. 1c,d) (Bray et al., 1983; Duncan et al., 1983; Griffiths et al., 1981a, 1981b). Axonal caliber increases with age in *sh* pup and no difference between the axonal diameters of affected and age-matched normal pups was found (Bray et al., 1983; Duncan et al., 1983; Griffiths et al., 1981a, 1981b). The myelination defect is always more severe in the cerebral white matter and optic nerves than in the spinal cord (Bray et al., 1983; Duncan et al., 1983; Griffiths et al., 1981a, 1981b). The availability of myelinated and hypomyelinated tissue in control and *sh* pups respectively presents a unique opportunity to study parameters of the two-pool model of MT free from the confounding effects of other pathological substrates, such as inflammation and axon loss.

Materials and methods

MRI protocol

The data were acquired on a 3T GE SIGNA scanner (General Electric Healthcare, Waukesha, Wisconsin, USA). Six *sh* pups (S1–S6) and four age-matched control dogs (C1–C4) were scanned at ages ranging between 3 and 21 months (time points, in months: S1—3.5, 8; S2—4; S3—5.2, 10, 21; S4—5.7; S5—7, 15.5; S6—13; C1—3, 15; C2—4, 5.5, 14; C3—5, 9; C4—10). The animals were anesthetized and imaged with a single-channel, quadrature T/R extremity coil. The protocol included collection of MT-weighted data, variable flip angle (VFA) data for longitudinal relaxation rate (R_1) and equilibrium magnetization (M_0) mapping (Deoni et al., 2003; Wang et al., 1987), and data for double flip angle B_1 mapping (Insko and Bolinger, 1993; Wang et al., 2005). We used a 3D TOF SPGR-based sequence for acquisition of MT and VFA datasets (image matrix size $256\times192\times60$, FOV = 15 cm, slice thickness 1.6 mm). MT imaging was performed in a pulsed regime, with MT pulse played in every T_R (8 ms Fermi pulse, $T_R/T_E = 38/3.6$ ms, flip = 10°). MT datasets were acquired at the following combinations of offset frequencies Δ and effectual flip angles of MT saturation pulse: 3 kHz/850° (2NEX), 3 kHz/500°, 6 kHz/850°, 6 kHz/500° (2NEX), 9 kHz/850°, 9 kHz/500°, 16 kHz/850°, 20 kHz/500°. The same imaging pulse sequence was used to collect an additional dataset without MT saturation. Two VFA datasets were collected with the same imaging sequence with flip angles of 4° (proton density weighted) and 23° (T_1-weighted) ($T_R = 21$ ms). The data for B_1 mapping were collected using multi-shot SE EPI sequence ($T_R/T_E = 10{,}000/14.8$ ms, image matrix 96×96, FOV = 15 cm,

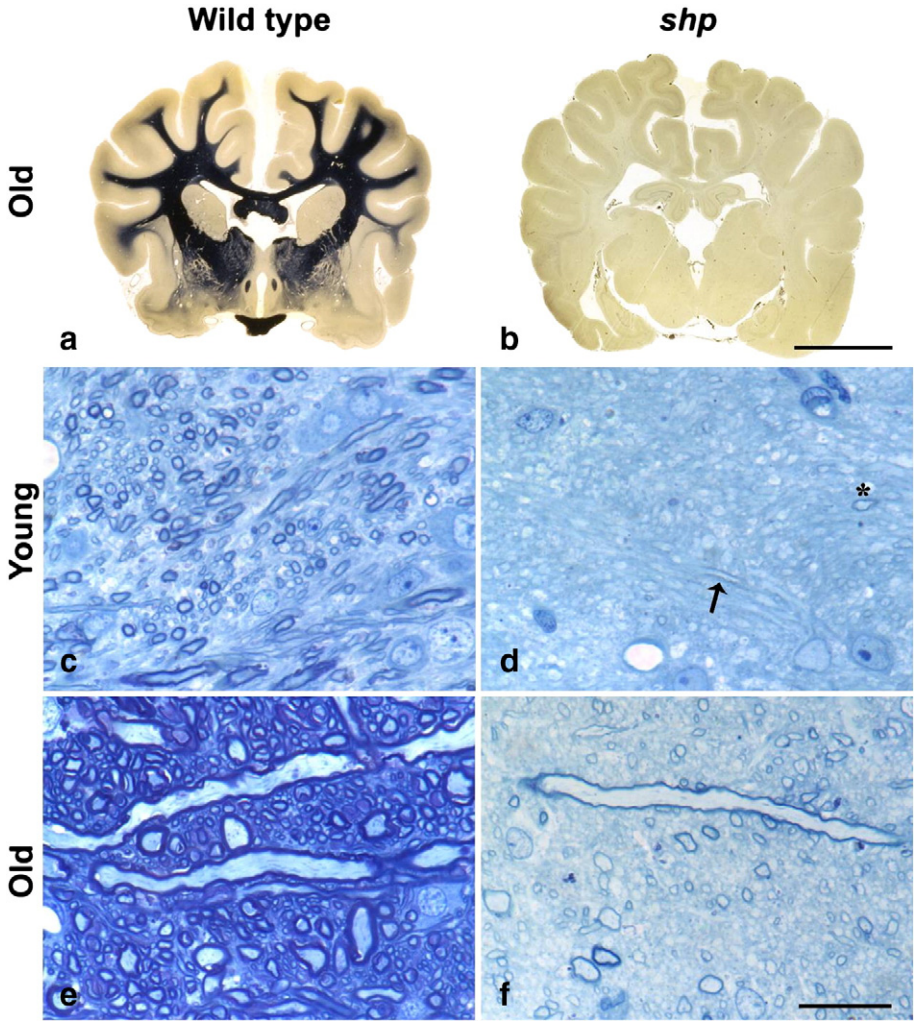

Fig. 1. Lack of myelination in the brain of the shaking pup: a, b. Whole brain stained for myelin from a 1 year old normal dog, a) and a *sh* pup b). The internal capsule from a 4 week old normal dog c) and a 5 week old *sh* pup d) and 1 yr 2 month old normal dog e) and 1 yr 3 month old *sh* pup f). In the normal dog there is an increase in axon size and myelin density from 1 month to 1 yr (c, e). In the *sh* pup at 5 weeks of age, only two myelin profiles can be seen (arrow) and one axon cut on transverse section (asterisk) d). In contrast, in the older *sh* pup, more myelin is present but the sheaths are thin (both those sectioned longitudinally and transversely) and the myelin density is much less than in the control (e). a, b. Heidenhain stain; scale bar = 1 cm. c–f. Toluidine blue stained, 1 micron sections, scale bar = 20 μm. Tissue for representative histology was collected following intravascular perfusion with either 4% paraformaldehyde or 2.5% glutaraldehyde. The brain was embedded in celloidin for sectioning and whole-brain Heidenhain staining for myelin. A similar area was dissected from the internal capsule of young and old control dogs and shaking pups, and embedded in plastic for sectioning at 1-micron thickness and staining with Toluidine blue.

slice thickness 3.2 mm, 30 slices) with two sets of flip and refocusing angles (60°/120° and 120°/240°). High-order shimming was applied before the scans to minimize inhomogeneity of main magnetic field B_0 over the brain.

Data processing and estimation of parametric maps

Brain volume was extracted from a T_1-weighted image using brain extraction tool followed by semiautomatic contouring (Jim 5.0 Software, Xinapse Systems Ltd, UK). All other datasets were co-registered to the brain volume using FLIRT image registration tool (FSL; FMRIB, Oxford, UK). B_1 error maps were estimated as described in Wang et al. (2005). The B_1 error map represents a spatially varying scaling factor between the nominal B_1 value and the actual one, and may be used to correct regional variations in both MT pulse and excitation flip angles, which should increase the accuracy of parameter estimation. The B_1 error maps were used to scale nominal MT pulse value and excitation flip angle values pixelwise before passing them to the estimation routine. As B_0 variations were minimized through high-order shimming, B_0 was assumed uniform in the calculations. R_1 and M_0 maps were estimated for fitting the VFA data to the SPGR signal equation

$$S = M_0 \cdot \sin\alpha \frac{1-e^{-T_R R_1}}{1-e^{-T_R R_1}\cos\alpha} \quad (1)$$

using non-linear least squares minimization. MT data were first normalized by the image without MT saturation and then were fitted to the first-order analytical approximation to the expression for steady-state magnetization in pulsed MT experiments based on SPGR sequences (Yarnykh and Yuan, 2004) using non-linear least squares. We assumed that the direct saturation effect of MT pulse on the free pool is negligible at the off-resonance frequencies of MT pulses used, which was shown to be a valid assumption for off-resonance frequencies >2.5 kHz (Portnoy and Stanisz, 2007; Yarnykh, 2002). This allowed excluding transverse relaxation time T_2 of the free pool from estimation. All data-fitting routines were implemented in Matlab environment on a standard PC. The qMT code is available as a part of qMAP software package (http://www.

medphysics.wisc.edu/~samsonov/qmap/). Additionally, traditional MT ratio was calculated using images with (MT_{ON}, MT flip = 850°, Δ = 3 kHz) and without (MT_{OFF}) the MT pulse:

$$MTR = \frac{MT_{OFF} - MT_{ON}}{MT_{OFF}}. \quad (2)$$

Brain-masked R_1 maps and the MT_{ON} image were supplied to the FAST tool (FSL; FMRIB, Oxford, UK) for three-class segmentation (WM/GM/CSF). The MT-weighted image was required to allow robust CSF segmentation, especially for the *sh* pups where T_1 contrast between WM and CSF was not sufficient to robustly classify these tissues. The resulting partial volume maps were thresholded at the 0.95 level to yield WM/GM maps with minimized partial volume effect. Additionally, individual regions of interest (ROI) were identified on T_1-w SGPR images. To assess the most compact white matter, WM ROI were placed in the bilateral internal capsules. Gray matter (GM) ROI were placed in caudate nucleus (Fig. 2). CSF ROI were placed in ventricles in close proximity to the GM/WM ROIs.

To assess tissue water content, we estimated a normalized proton density map (PD_n) from M_0 maps. M_0 is proportional to free proton density *PD*. However, its utility as a measure of water proton density in longitudinal studies is limited by a number of technical factors including coil sensitivity (C), the hardware/image reconstruction gain (g), and relaxation time (T_2^*):

$$M_0 = g \cdot C \cdot PD \cdot e^{-T_E/T_2^*}. \quad (3)$$

Among those factors, the coil sensitivity modulation is not trivial to correct, as it depends on coil loading and positioning of the subject in the coil. In this paper, we extend the CSF-based MT normalization approach of Smith et al. (2005) to derive a more stable measure of proton density. In that paper, MT-insensitive CSF signal surrounding spinal cord was used to obtain a system-independent measure of magnetization transfer within the cord. In our approach, we use the mean value of signal within CSF, $\hat{M}_0^{(CSF)}$, ROI to remove system and coil dependencies:

$$PD_n = \frac{M_0}{\hat{M}_0^{(CSF)}} \approx \frac{PD}{PD^{(CSF)}}. \quad (4)$$

The expression may be derived from Eq. (3) making the assumptions that $T_2^* \gg T_E$ and that coil sensitivity values do not change significantly in the area of ROI placements. The former assumption is valid for the range of echo times used in the study. We found that the latter assumption holds well in our experiments because the spatial profile of the T/R birdcage coil used in the study is very uniform over the dog's brain.

Statistical analysis

Weighted least squares was used to test for differences in each of the qMT parameters. The ROI SD squared reciprocal was used as inverse variance weights. To study differences between control and *sh* pups, two variants of the model were fitted: Model 1 has experimental group as the independent variable; Model 2 adds age and the group by age interaction. This parameterization corresponds to fitting straight lines to the healthy and *sh* group,

$$\text{Parameter} = \beta_{1,i} * \text{age} + \beta_{0,i} + \text{noise}, \quad i \in \{\text{Control}, \text{Sh}\} \quad (5)$$

while allowing for testing of whether the intercepts or slopes differ between groups, as well as testing the significance of age-related (difference from zero) effects only. Pearson correlations were obtained separately for each group. Diagnostic plots were obtained to assess possible violations in model assumptions. Gray and white matter regions were analyzed separately. The significance of parameters in the linear models was tested based on the ANOVA table. Statistical

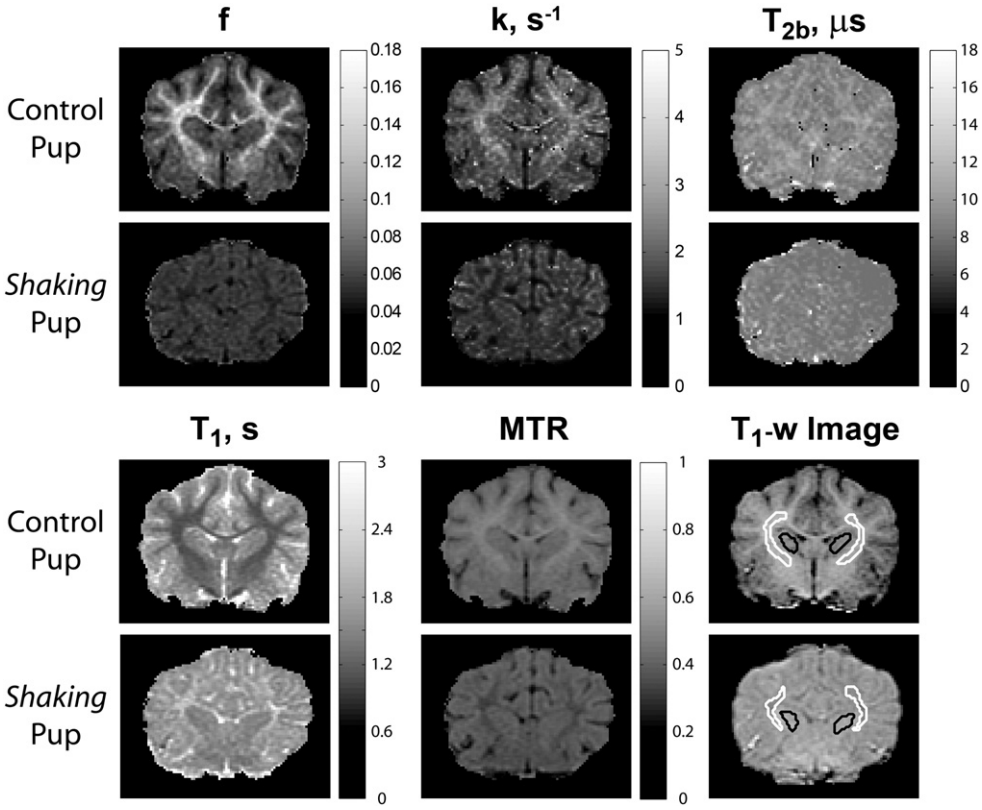

Fig. 2. Representative parametric maps in *sh* pup and normal dog and anatomical T_1-weighted image with ROIs (white — WM; black — GM).

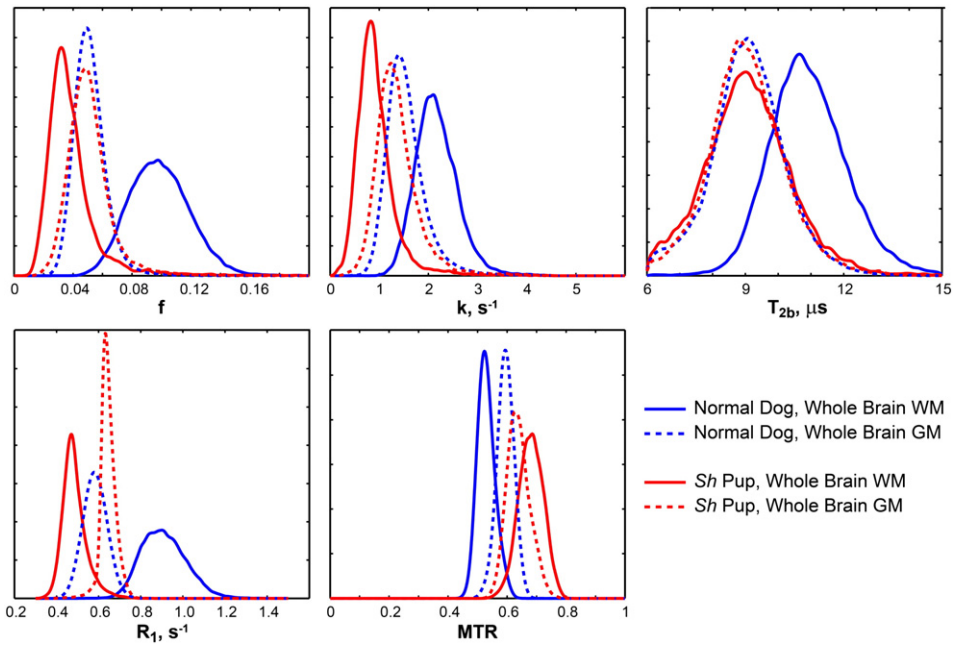

Fig. 3. Representative distributions of quantitative parameters in white matter (WM) and gray matter (GM) of *sh* pup and normal dog (4 months of age).

significance was assessed at a *p*-value less than 0.05. The statistical analysis was generated in R 2.12.1 (R Development Core Team, 2009).

Results

Representative parametric maps in myelinated and hypomyelinated dogs are shown in Fig. 2. The absence of myelin sheaths is apparently reflected by markedly decreased bound pool fraction *f* in the *sh* pup. The WM/GM contrast appears reversed on *f* maps between control and *sh* pups. This observation is in accordance with the reversed WM/GM contrast seen on histological myelin stains in the *sh* pup (Fig. 1b). Reversed gray-white contrast is also observed on *k*, $T_1 = 1/R_1$, and *MTR* maps. Mild gray-white contrast is seen on the T_{2b} map for the control dog while none is distinguishable on the T_{2b} map for the *sh* pup. These effects also can be observed on representative normalized histograms of qMT measures in WM and GM from whole brain segmentation (Fig. 3). The WM distributions are clearly separated between control and mutant animals for all parameters. For GM, the separation is most pronounced for *k*, R_1, and *MTR* and least seen for *f* and T_{2b}. The age-related effects on these parameters are discussed in the next paragraphs.

These qualitative observations are further supported by quantitative measurements in Table 1. Table 1 shows means and standard deviations of quantitative parameters in WM/GM ROIs and group differences taken across all ages. Statistically significant differences between controls and *sh* pups were observed for all measures in both WM and GM ROIs. The putative myelin-related parameter *f* was the most distinctive between *sh* pups and controls, as expected from the profound paucity of myelin in the *sh* pup. Simultaneously, hypomyelinated WM shows marked reduction in *k* and to a lesser degree in T_{2b}, which may reflect different compartmental organization of the hypomyelinated WM (see Discussion). R_1 in WM also provides excellent discrimination between *sh* pups and controls; proton density values are increased by 32% in *sh* pup WM, which likely indicates increased extracellular water content in the absence of myelin sheaths. This increased amount of free water also may be responsible for the observed 75% decrease in R_1 (see Discussion). The effect size between control and sh pups were much smaller in GM than in WM for all parameters.

The plots in Figs. 4 and 5 show the age-related changes of qMT measures, MTR, and PD_n in control and mutant animals and linear regression curves from statistical analysis. The effect of normalization

Table 1
Means and standard deviations of qMT measures and group differences between controls and *sh* pups.

	ROI-IC					ROI-CN				
	Control	*Sh*	Δ (p-value)	R^2 (RSE)	ES, %	Control	*Sh*	Δ (p-value)	R^2 (RSE)	ES, %
f	0.121 ± 0.004	0.031 ± 0.004	**0.090** (<10^{-4})	0.971 (0.599)	**118**	0.0536 ± 0.0020	0.0455 ± 0.0024	**0.0081** (4.04e^{-3})	0.413 (0.609)	**16**
k (s^{-1})	2.547 ± 0.055	0.825 ± 0.062	**1.722**(<10^{-4})	0.980 (0.396)	**102**	1.613 ± 0.059	1.298 ± 0.073	**0.315** (4.97e^{-4})	0.257 (0.542)	**22**
T_2 (μs)	11.09 ± 0.19	8.930 ± 0.260	**2.160** (<10^{-4})	0.810 (0.521)	**22**	9.855 ± 0.16	9.235 ± 0.206	**0.650** (7.16e^{-3})	0.417 (0.482)	**7**
R_1 (s^{-1})	1.051 ± 0.029	0.471 ± 0.031	**0.580** (<10^{-4})	0.956 (0.887)	**76**	0.673 ± 0.016	0.630 ± 0.019	**0.043** (0.014)	0.303 (0.726)	**7**
PD_n	0.597 ± 0.010	0.827 ± 0.014	**−0.230** (<10^{-4})	0.947 (0.911)	**32**	0.755 ± 0.011	0.787 ± 0.01340	**−0.0323** (0.0283)	0.267 (0.959)	**3**
MTR	0.496 ± 0.004	0.305 ± 0.006	**0.191** (<10^{-4})	0.985 (0.542)	**48**	0.404 ± 0.006	0.364 ± 0.008	**0.040** (<10^{-4})	0.629 (0.815)	**10**

Δ = control − sh

$$\text{Effect Size}(ES) = \frac{|\text{control} - \text{sh}|}{0.5 \cdot (\text{control} + \text{sh})} \cdot 100\%$$

RSE — Residual standard error.
Bold font indicates statistically significant results (p<0.05).
IC = internal capsules (WM); CN = caudate nuclei (GM).

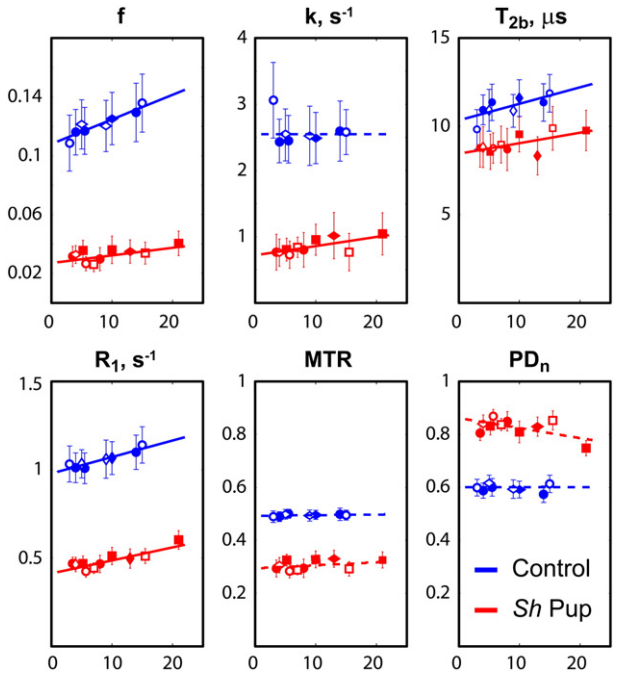

Fig. 4. Plots of quantitative MT measures across ages in white matter of *sh* pups and control dogs. The measurements were taken across 3D ROIs at the bilateral internal capsules. Horizontal axes correspond to age in weeks. Each symbol denotes an individual pup. Solid lines correspond to slopes of fitted lines significantly different from zero (Table 2).

on PD_n may be appreciated by comparing the PD_n plots for IC and CN ROI (Figs. 4 and 5, respectively) with the corresponding plots based on uncorrected M_0 (Fig. 6). Table 2 shows the results of linear fitting to the age-related data. In the internal capsules, slopes were significantly different from zero for f, T_{2b} and R_1 in controls and for f, k, T_{2b} and R_1 in the *sh* pups. In caudate nuclei, the slopes were statistically

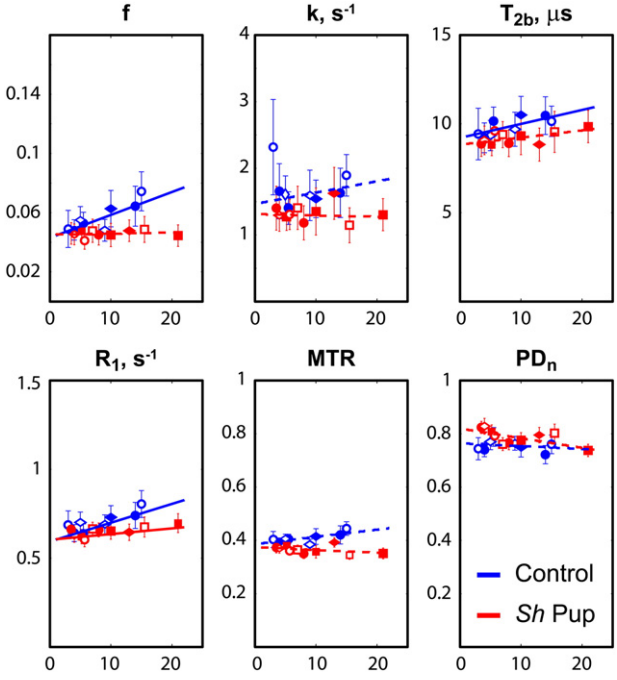

Fig. 5. Plots of quantitative MT measures across ages in gray matter of *sh* pups and control dogs. The measurements were taken across 3D ROIs at the bilateral caudate nuclei. Horizontal axes correspond to age in months. Each symbol denotes an individual pup. Solid lines correspond to slopes of fitted lines significantly different from zero (Table 2).

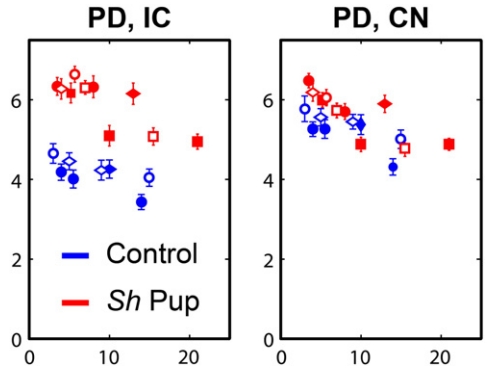

Fig. 6. Uncorrected proton density values in WM IC and GM CN ROIs. Horizontal axes correspond to age in months. Each symbol denotes an individual pup.

significant for f, T_{2b} and R_1 in controls and R_1 in the *sh* pups. In control dogs, the bound pool fraction f progressively increased during the studied period in WM of control dogs. T_{2b} and R_1 also significantly increased with age in controls and the age-related changes of parameter f strongly correlated with those of T_{2b} ($R=0.824$, $p=0.0063$) and R_1 ($R=0.843$, $p=0.00435$). At the same time, the relative age-related changes of bound pool fraction in WM of normal dog were the greatest of the three ($\beta_1(f)/<f>=13.8e-3$, $\beta_1(T_{2b})/<T_{2b}>=8.4e-3$, $\beta_1(R_1)/<R_1>=8.9e-3$, where $< >$ is a mean value). The differences in the age-related changes as revealed by the slopes were not statistically significant between control and *sh* pup groups in all cases, except in GM ROI for f and *MTR*; however, the slopes for the *sh* pup group were also not statistically different from zero in these cases.

Discussion

We presented results of two-pool MT modeling of global and age-related differences in myelination between the myelin mutant *sh* pup and age-matched controls. The *sh* pup is a "reductionist" disease model (Dubois-Dalcq et al., 2005) that presents a needed opportunity to study imaging markers of myelin disease free from confounding changes of inflammation, edema, and axonal loss, which are commonly seen in other animal models. All qMT measures were sensitive to differences between normally myelinated and hypomyelinated WM tissues. Among them, bound pool fraction f was found to be the most discriminating parameter ($ES=118\%$). MTR, the traditional measure of the MT effect, showed differences on a much smaller scale than did f ($ES=48\%$). Given that profound hypomyelination is the primary manifestation of the PLP gene mutation in the *sh* pup, the observed reduction in f may be attributed to severe paucity of myelin in the affected animal.

The observed qMT parameter changes also extended to the GM on ROI analysis, though less pronounced than in the WM. This result is not unexpected given that GM normally contains some myelin and that the PLP mutation impacts myelin synthesis globally. The ability to detect myelin abnormalities in GM has particular relevance for MS, in which disease in the GM has recently become the focus of intensive study by the MS research community (Pirko et al., 2007).

No significant age-related changes in MTR were found in normal dogs, which may reflect the fact that this traditional measure of the MT effect, while sensitive to myelin content, has previously been shown to have limited specificity to myelin (Does et al., 1998; Mottershead et al., 2003); given this lack of specificity, there may have been tissue features changing in concert with myelination that had an offsetting influence on MTR (see argument regarding opposing MT and T_1 effects below). Another possibility is that the level of MTR changes may be too small to be statistically significant with the number of animals used in the current study.

Table 2
Results of linear regression analyses for all qMT measures in internal capsules and caudate nucleus vs. age and group for control dogs and *sh* pups.

		ROI-IC (Estimate ± SE (*p*-value))			ROI-CN (Estimate ± SE (*p*-value))		
		Control	*Sh*	R^2 (RSE)	Control	*Sh*	R^2 (RSE)
f	β_0	**0.108 ± 0.006 (<10^{-4})**	**0.027 ± 0.002 (<10^{-4})***	0.984 (0.475)	**0.043 ± 0.003 (<10^{-4})**	**0.045 ± 0.002 (<10^{-4})**	0.688 (0.475)
	β_1	**1.671e − 3 ± 0.728e − 3 (0.038)**	**0.519e − 3 ± 0.209e − 3 (0.026)**		**1.548e − 3 ± 0.442e − 3 (0.036)**	0.0682e − 3 ± 0.205e − 3 (0.744)*	
k (s^{-1})	β_0	**2.547 ± 0.108 (<10^{-4})**	**0.718 ± 0.052 (<10^{-4})***	0.986 (0.358)	**1.467 ± 0.141 (<10^{-4})**	**1.313 ± 0.082 (<10^{-4})**	0.583 (0.516)
	β_1	2.886e − 5 ± 1.156e − 2 (0.998)	**1.383e − 2 ± 0.582e − 2 (0.033)**		0.017 ± 0.015 (0.269)	− 0.002 ± 0.008 (0.831)	
T_2 (μs)	β_0	**1.034e − 5 ± 0.032e − 5 (<10^{-4})**	**0.845e − 5 ± 0.028e − 5(<10^{-4})***	0.897 (0.410)	**0.921e − 5 ± 0.03e − 5 (<10^{-4})**	**0.883e − 5 ± 0.02 e − 5 (<10^{-4})**	0.657 (0.405)
	β_1	**9.339e − 8 ± 3.53e − 8 (0.019)**	**5.943e − 8 ± 2.69e − 8 (0.045)**		**7.863e − 8 ± 3.2e − 8 (0.019)**	3.992e − 8 ± 2.091e − 8 (0.077)	
R_1 (s^{-1})	β_0	**0.979 ± 0.036 (<10^{-4})**	**0.412 ± 0.013 (<10^{-4})***	0.987 (0.514)	**0.593 ± 0.024 (<10^{-4})**	**0.603 ± 0.014 (<10^{-4})**	0.678 (0.510)
	β_1	**9.325e − 3 ± 4.079e − 3 (0.038)**	**7.379e − 3 ± 1.383e − 3(1.1e − 4)**		**1.06e − 2 ± 0.28e − 2 (2.4e − 3)**	**0.32e − 2 ± 0.015e − 2 (0.048)***	
PD_n	β_0	**0.602 ± 0.018 (<10^{-4})**	**0.861 ± 0.015 (<10^{-4})***	0.965 (0.792)	**0.763 ± 0.019 (<10^{-4})**	**0.820 ± 0.012 (<10^{-4})***	0.571 (0.783)
	β_1	− 0.584e − 4 ± 2.06e − 4 (0.781)	− 37.72e − 4 ± 11.18e − 4 (0.019)		− 1.05e − 3 ± 2.18e − 3 (0.64)	− 3.605e − 3 ± 1.15e − 3 (7.59e − 3)	
MTR	β_0	**0.494 ± 0.008 (<10^{-4})**	**0.295 ± 0.009 (<10^{-4})***	0.986 (0.549)	**0.386 ± 0.012 (<10^{-4})**	**0.374 ± 0.009 (<10^{-4})**	0.7221 (0.753)
	β_1	2.470e − 4 ± 9.161e − 4 (0.791)	11.5e − 4 ± 9.41e − 4 (0.240)		2.73e − 3 ± 1.535e − 3(0.458)	− 1.04e − 3 ± 0.84e − 3 (0.233)*	

RSE — Residual standard error.
Bold font indicates results that were statistically significant ($p<0.05$). Asterisk (*) indicates results where the difference of slope/intercept for the *sh* pup was statistically significant compared to control dogs.
The age of pups ranges from 3 to 21 months.

Bound pool fraction, which relies on more sophisticated and time demanding data acquisition and processing than MTR, showed a significant increase with age, which may indicate that it is sufficiently sensitive and specific to track normal myelin development even in the face of other tissue changes occurring simultaneously (e.g. axon size, free water content). Note, however, that specificity cannot reliably be ascertained from correlation alone; therefore, this remains speculative.

Remarkably, longitudinal relaxation rate R_1 is markedly decreased in *sh* pup WM (ES = 76%). Since axons are known to be relatively well preserved in the mutant (Bray et al., 1983; Duncan et al., 1983; Griffiths et al., 1981a, 1981b), this observation suggests that, despite previously reported associations between T_1 relaxation and axonal count/density [e.g. (Mottershead et al., 2003; van Walderveen et al., 1998)], T_1 is not specific for axons and cannot serve as an axonal marker. The observed R_1 increase with age in control dogs and strong correlation with age-related changes in bound pool fraction support the hypothesis that R_1 may be biologically correlated (and T_1 inversely correlated) with level of myelination (Mottershead et al., 2003). One possible mechanism is through compartmental WM changes such as changes in amount of intercellular water with myelin content. This observation is also supported by the fact that free water content as measured by PD_n was also significantly decreased in control dogs (ES = 32%). This correlation may also explain the absence of age-related changes in MTR in normal dogs. As discussed in Underhill et al. (2011) and Yarnykh (2002), in typical magnetization transfer experiments, MTR is inversely proportional to a weighted sum of $(fT_1)^{-1}$ and $(kT_1)^{-1}$. T_1 is an indirect measure of extracellular water content, which decreases with myelination while macromolecular content (reflected by f) increases, resulting in opposing effects on MTR, which may reduce its specificity with respect to the individual components. This reasoning is also along the line of recent study of healthy brains, which has shown that the overall effect on MTR from an increase (decrease) in relaxation times may be counterbalanced with a decrease (increase) in MT parameters (Garcia et al., 2012). We conclude that even though R_1 is not directly associated with any particular water compartment, it may be a useful parameter in combination with other, more specific parameters. For example, in seeking effects that are independent from changes in overall water content, R_1 might be useful as a covariate representing free water in a multivariate analysis.

Specificity of pool size ratio to axonal content was studied by Ou et al. (2009b) where it was found to be insensitive to axonal degeneration in injured optic nerve in both normal and myelin-deficient *shiverer* mice, supporting its association with the myelin pool. At the same time, the observed pool size ratio differences between normal and myelin-deficient tissues were moderate (ES = 39%, calculated from pool size ratio values from Table 1 in Ref. (Ou et al., 2009b) for left optic nerve), implying that semisolid tissue components other than myelin and axonal membranes may be significant contributors to the measured amount of bound protons. As mentioned above, our study revealed more dramatic changes in bound pool size (ES = 118%). Given that axons are preserved in the *sh* pup (Bray et al., 1983; Duncan et al., 1983; Griffiths et al., 1981a, 1981b), our study may serve as independent confirmation of the high specificity and sensitivity of f to myelination. The difference between the studies may be related to residual myelination levels in the respective animal models, anatomical features (brain vs. optic nerve), or respective methods used to quantify bound pool size.

Based on our measurements, the size of the bound pool in the hypomyelinated animal is about 26% of the bound pool in the normal dog. More complex models of the MT effect include several semisolid and free pools to distinguish between myelin and non-myelin semisolid pools, which makes biological sense. In particular, several studies (Bjarnason et al., 2005; Levesque and Pike, 2009; Stanisz et al., 1999) proposed four-pool models with two semisolid pools (myelin and non-myelin tissue) and two free proton pools (myelin water and intra-/extra-cellular [IE] water), each free pool being in magnetization exchange with its corresponding semisolid pool and with each other. Given the significantly different composition of bound pools in the *sh* pups (non-myelin protons) and control dogs (non-myelin and myelin protons), the hypomyelinated animal in our study may to some degree be considered a biological approximation to the four-pool model, where the size of the semisolid pool associated with myelin is diminished. T_{2b} was decreased in the hypomyelinated animals (ES = 22%), similar to the decrease of T_{2b} previously seen in MS lesions (Sled and Pike, 2001; Yarnykh, 2002). T_{2b} also showed significant age-related changes in control dogs, which showed significant positive correlation with f. This indicates that myelination increases the effective T_{2b} as measured by the two-pool model and that myelin and non-myelin pools are characterized by different T_{2b} values. Along the same lines, the observed change in cross-relaxation rate k

between control and *sh* pups (ES = 102%) may indicate that cross-relaxation between non-myelin tissue and IE water is much slower than the measured cross-relaxation rate in the presence of myelinated tissue. This is consistent with bovine optic nerve studies using a four-pool MT model where the exchange rate between IE water and non-myelin tissue was found to be significantly slower than between the myelin water compartment and myelin (Bjarnason et al., 2005). While four-pool models may improve specificity of quantitative MT imaging, their application in vivo is impeded by the lack of practical imaging methods and potentially long imaging times needed to estimate the extended set of parameters. The observed changes in key parameters governing MT effects suggest that both non-myelin and myelin bound protons potentially may be distinguished using pulse sequences/experimental designs aimed to exploit the differences in k and T_{2b}.

Significant limitations of the study include the relatively small number of dogs, necessitated by the greater cost and ethical concerns relative to studies in rodents, and the lack of direct voxel-for-voxel co-localization between MRI and histomorphometric data, which we were unable to achieve reliably given the marked discrepancies of scale between MR images and micrographs. However, the pathologic features of the disease have been remarkably consistent across animals in our experience and have shown very limited regional variations within such specific structures as the internal capsule.

Conclusions

This study demonstrates the limitations inherent in traditional magnetization transfer (MT) contrast using the MT ratio (MTR), which provides a misleading characterization of pathology even in a reductionist white matter disease model lacking inflammation or axon loss. Quantitative MT (qMT) imaging provides a more accurate and potentially more specific non-invasive tissue characterization and, though it is more complex and time-consuming, it is nevertheless feasible to acquire on clinical platforms and should be further investigated as a source of imaging markers to support research in MS and other white matter diseases.

Acknowledgments

The authors would like to thank Dr. Alejandro Munoz Del Rio for assistance with statistical analysis. This work was supported by NIH NINDS (R01NS050466, R01NS065034) and a Translational Research Partnership Grant from the National Multiple Sclerosis Society (TR-3761).

References

Bjarnason, T.A., Vavasour, I.M., Chia, C.L., MacKay, A.L., 2005. Characterization of the NMR behavior of white matter in bovine brain. Magn. Reson. Med. 54, 1072–1081.
Blezer, E.L., Bauer, J., Brok, H.P., Nicolay, K., t Hart, B.A., 2007. Quantitative MRI-pathology correlations of brain white matter lesions developing in a non-human primate model of multiple sclerosis. NMR Biomed. 20, 90–103.
Bray, G.M., Duncan, I.D., Griffiths, I.R., 1983. 'Shaking pups': a disorder of central myelination in the spaniel dog. IV. Freeze-fracture electron microscopic studies of axons, oligodendrocytes and astrocytes in the spinal cord white matter. Neuropathol. Appl. Neurobiol. 9, 369–378.
Davies, G.R., Tozer, D.J., Cercignani, M., Ramani, A., Dalton, C.M., Thompson, A.J., Barker, G.J., Tofts, P.S., Miller, D.H., 2004. Estimation of the macromolecular proton fraction and bound pool T2 in multiple sclerosis. Mult. Scler. 10, 607–613.
Deloire-Grassin, M.S., Brochet, B., Quesson, B., Delalande, C., Dousset, V., Canioni, P., Petry, K.G., 2000. In vivo evaluation of remyelination in rat brain by magnetization transfer imaging. J. Neurol. Sci. 178, 10–16.
Deoni, S.C., Rutt, B.K., Peters, T.M., 2003. Rapid combined T1 and T2 mapping using gradient recalled acquisition in the steady state. Magn. Reson. Med. 49, 515–526.
Does, M.D., Beaulieu, C., Allen, P.S., Snyder, R.E., 1998. Multi-component T1 relaxation and magnetisation transfer in peripheral nerve. Magn. Reson. Imaging 16, 1033–1041.
Dousset, V., Brochet, B., Vital, A., Gross, C., Benazzouz, A., Boullerne, A., Bidabe, A.M., Gin, A.M., Caille, J.M., 1995. Lysolecithin-induced demyelination in primates: preliminary in vivo study with MR and magnetization transfer. AJNR Am. J. Neuroradiol. 16, 225–231.
Dubois-Dalcq, M., Ffrench-Constant, C., Franklin, R.J., 2005. Enhancing central nervous system remyelination in multiple sclerosis. Neuron 48, 9–12.
Dula, A.N., Gochberg, D.F., Valentine, H.L., Valentine, W.M., Does, M.D., 2010. Multi-exponential T2, magnetization transfer, and quantitative histology in white matter tracts of rat spinal cord. Magn. Reson. Med. 63, 902–909.
Duncan, I.D., Griffiths, I.R., Munz, M., 1983. 'Shaking pups': a disorder of central myelination in the spaniel dog. III. Quantitative aspects of glia and myelin in the spinal cord and optic nerve. Neuropathol. Appl. Neurobiol. 9, 355–368.
Garcia, M., Gloor, M., Radue, E.W., Stippich, C., Wetzel, S.G., Scheffler, K., Bieri, O., 2012. Fast high-resolution brain imaging with balanced SSFP: interpretation of quantitative magnetization transfer towards simple MTR. Neuroimage 59, 202–211.
Gass, A., Barker, G.J., Kidd, D., Thorpe, J.W., MacManus, D., Brennan, A., Tofts, P.S., Thompson, A.J., McDonald, W.I., Miller, D.H., 1994. Correlation of magnetization transfer ratio with clinical disability in multiple sclerosis. Ann. Neurol. 36, 62–67.
Gochberg, D.F., Gore, J.C., 2003. Quantitative imaging of magnetization transfer using an inversion recovery sequence. Magn. Reson. Med. 49, 501–505.
Gochberg, D.F., Kennan, R.P., Robson, M.D., Gore, J.C., 1999. Quantitative imaging of magnetization transfer using multiple selective pulses. Magn. Reson. Med. 41, 1065–1072.
Griffiths, I.R., Duncan, I.D., McCulloch, M., 1981a. Shaking pups: a disorder of central myelination in the spaniel dog. II. Ultrastructural observations on the white matter of the cervical spinal cord. J. Neurocytol. 10, 847–858.
Griffiths, I.R., Duncan, I.D., McCulloch, M., Harvey, M.J., 1981b. Shaking pups: a disorder of central myelination in the Spaniel dog. Part 1. Clinical, genetic and light-microscopical observations. J. Neurol. Sci. 50, 423–433.
Hickman, S.J., Toosy, A.T., Jones, S.J., Altmann, D.R., Miszkiel, K.A., MacManus, D.G., Barker, G.J., Plant, G.T., Thompson, A.J., Miller, D.H., 2004. Serial magnetization transfer imaging in acute optic neuritis. Brain 127, 692–700.
Insko, E.K., Bolinger, L., 1993. Mapping of the radiofrequency field. J. Magn. Reson. A 103, 82–85.
Kimura, H., Grossman, R.I., Lenkinski, R.E., Gonzalez-Scarano, F., 1996. Proton MR spectroscopy and magnetization transfer ratio in multiple sclerosis: correlative findings of active versus irreversible plaque disease. AJNR Am. J. Neuroradiol. 17, 1539–1547.
Kucharczyk, W., Macdonald, P.M., Stanisz, G.J., Henkelman, R.M., 1994. Relaxivity and magnetization transfer of white matter lipids at MR imaging: importance of cerebrosides and pH. Radiology 192, 521–529.
Levesque, I.R., Pike, G.B., 2009. Characterizing healthy and diseased white matter using quantitative magnetization transfer and multicomponent T(2) relaxometry: a unified view via a four-pool model. Magn. Reson. Med. 62, 1487–1496.
Levesque, I., Sled, J.G., Narayanan, S., Santos, A.C., Brass, S.D., Francis, S.J., Arnold, D.L., Pike, G.B., 2005. The role of edema and demyelination in chronic T1 black holes: a quantitative magnetization transfer study. J. Magn. Reson. Imaging 21, 103–110.
Loevner, L.A., Grossman, R.I., McGowan, J.C., Ramer, K.N., Cohen, J.A., 1995. Characterization of multiple sclerosis plaques with T1-weighted MR and quantitative magnetization transfer. AJNR Am. J. Neuroradiol. 16, 1473–1479.
MacKay, A., Whittall, K., Adler, J., Li, D., Paty, D., Graeb, D., 1994. In vivo visualization of myelin water in brain by magnetic resonance. Magn. Reson. Med. 31, 673–677.
Mottershead, J.P., Schmierer, K., Clemence, M., Thornton, J.S., Scaravilli, F., Barker, G.J., Tofts, P.S., Newcombe, J., Cuzner, M.L., Ordidge, R.J., McDonald, W.I., Miller, D.H., 2003. High field MRI correlates of myelin content and axonal density in multiple sclerosis—a post-mortem study of the spinal cord. J. Neurol. 250, 1293–1301.
Nadon, N.L., Duncan, I.D., 1996. Molecular analysis of glial cell development in the canine 'shaking pup' mutant. Dev. Neurosci. 18, 174–184.
Nadon, N.L., Duncan, I.D., Hudson, L.D., 1990. A point mutation in the proteolipid protein gene of the 'shaking pup' interrupts oligodendrocyte development. Development 110, 529–537.
Norton, W.T., Autilio, L.A., 1966. The lipid composition of purified bovine brain myelin. J. Neurochem. 13, 213–222.
Odrobina, E.E., Lam, T.Y., Pun, T., Midha, R., Stanisz, G.J., 2005. MR properties of excised neural tissue following experimentally induced demyelination. NMR Biomed. 18, 277–284.
Ou, X., Sun, S.W., Liang, H.F., Song, S.K., Gochberg, D.F., 2009a. The MT pool size ratio and the DTI radial diffusivity may reflect the myelination in shiverer and control mice. NMR Biomed. 22, 480–487.
Ou, X., Sun, S.W., Liang, H.F., Song, S.K., Gochberg, D.F., 2009b. Quantitative magnetization transfer measured pool-size ratio reflects optic nerve myelin content in ex vivo mice. Magn. Reson. Med. 61, 364–371.
Pierpaoli, C., Jezzard, P., Basser, P.J., Barnett, A., Di Chiro, G., 1996. Diffusion tensor MR imaging of the human brain. Radiology 201, 637–648.
Pirko, I., Lucchinetti, C.F., Sriram, S., Bakshi, R., 2007. Gray matter involvement in multiple sclerosis. Neurology 68, 634–642.
Portnoy, S., Stanisz, G.J., 2007. Modeling pulsed magnetization transfer. Magn. Reson. Med. 58, 144–155.
R Development Core Team, 2009. R: A Language and Environment for Statistical Computing. R Foundation for Statistical Computing, Vienna, Austria.
Rausch, M., Tofts, P., Lervik, P., Walmsley, A., Mir, A., Schubart, A., Seabrook, T., 2009. Characterization of white matter damage in animal models of multiple sclerosis by magnetization transfer ratio and quantitative mapping of the apparent bound proton fraction f. Mult. Scler. 15, 16–27.
Ropele, S., Seifert, T., Enzinger, C., Fazekas, F., 2003. Method for quantitative imaging of the macromolecular 1H fraction in tissues. Magn. Reson. Med. 49, 864–871.
Schmierer, K., Tozer, D.J., Scaravilli, F., Altmann, D.R., Barker, G.J., Tofts, P.S., Miller, D.H., 2007. Quantitative magnetization transfer imaging in postmortem multiple sclerosis brain. J. Magn. Reson. Imaging 26, 41–51.

Sled, J.G., Pike, G.B., 2001. Quantitative imaging of magnetization transfer exchange and relaxation properties in vivo using MRI. Magn. Reson. Med. 46, 923–931.
Smith, S.A., Golay, X., Fatemi, A., Jones, C.K., Raymond, G.V., Moser, H.W., van Zijl, P.C., 2005. Magnetization transfer weighted imaging in the upper cervical spinal cord using cerebrospinal fluid as intersubject normalization reference (MTCSF imaging). Magn. Reson. Med. 54, 201–206.
Stanisz, G.J., Kecojevic, A., Bronskill, M.J., Henkelman, R.M., 1999. Characterizing white matter with magnetization transfer and T(2). Magn. Reson. Med. 42, 1128–1136.
Stikov, N., Perry, L.M., Mezer, A., Rykhlevskaia, E., Wandell, B.A., Pauly, J.M., Dougherty, R.F., 2011. Bound pool fractions complement diffusion measures to describe white matter micro and macrostructure. Neuroimage 54, 1112–1121.
Tozer, D., Ramani, A., Barker, G.J., Davies, G.R., Miller, D.H., Tofts, P.S., 2003. Quantitative magnetization transfer mapping of bound protons in multiple sclerosis. Magn. Reson. Med. 50, 83–91.
Tozer, D.J., Davies, G.R., Altmann, D.R., Miller, D.H., Tofts, P.S., 2005. Correlation of apparent myelin measures obtained in multiple sclerosis patients and controls from magnetization transfer and multicompartmental T2 analysis. Magn. Reson. Med. 53, 1415–1422.
Underhill, H.R., Yuan, C., Yarnykh, V.L., 2009. Direct quantitative comparison between cross-relaxation imaging and diffusion tensor imaging of the human brain at 3.0 T. Neuroimage 47, 1568–1578.
Underhill, H.R., Rostomily, R.C., Mikheev, A.M., Yuan, C., Yarnykh, V.L., 2011. Fast bound pool fraction imaging of the in vivo rat brain: association with myelin content and validation in the C6 glioma model. Neuroimage 54, 2052–2065.
van Waesberghe, J.H., Kamphorst, W., De Groot, C.J., van Walderveen, M.A., Castelijns, J.A., Ravid, R., Lycklama a Nijeholt, G.J., van der Valk, P., Polman, C.H., Thompson, A.J., Barkhof, F., 1999. Axonal loss in multiple sclerosis lesions: magnetic resonance imaging insights into substrates of disability. Ann. Neurol. 46, 747–754.
van Walderveen, M.A., Kamphorst, W., Scheltens, P., van Waesberghe, J.H., Ravid, R., Valk, J., Polman, C.H., Barkhof, F., 1998. Histopathologic correlate of hypointense lesions on T1-weighted spin-echo MRI in multiple sclerosis. Neurology 50, 1282–1288.
Wang, H.Z., Riederer, S.J., Lee, J.N., 1987. Optimizing the precision in T1 relaxation estimation using limited flip angles. Magn. Reson. Med. 5, 399–416.
Wang, J., Qiu, M., Yang, Q.X., Smith, M.B., Constable, R.T., 2005. Measurement and correction of transmitter and receiver induced nonuniformities in vivo. Magn. Reson. Med. 53, 408–417.
Wolff, S.D., Balaban, R.S., 1989. Magnetization transfer contrast (MTC) and tissue water proton relaxation in vivo. Magn. Reson. Med. 10, 135–144.
Yarnykh, V.L., 2002. Pulsed Z-spectroscopic imaging of cross-relaxation parameters in tissues for human MRI: theory and clinical applications. Magn. Reson. Med. 47, 929–939.
Yarnykh, V.L., Yuan, C., 2004. Cross-relaxation imaging reveals detailed anatomy of white matter fiber tracts in the human brain. Neuroimage 23, 409–424.